Published in final edited form as:
*ACS Nano*. 2017 June 27; 11(6): 5753–5765. doi:10.1021/acsnano.7b01337.

# Agglomeration Determines Effects of Carbonaceous Nanomaterials on Soybean Nodulation, Dinitrogen Fixation Potential, and Growth in Soil

**Ying Wang**[†,‡,§], **Chong Hyun Chang**[⊥], **Dermont C. Bouchard**[‖], **Roger M. Nisbet**[‡,§,#], **Joshua P. Schimel**[‡,§,#], **Jorge L. Gardea-Torresdey**[§,▽], and **Patricia A. Holden**[*,†,‡,§]

[†]Bren School of Environmental Science and Management, University of California, Santa Barbara, CA 93106, United States

[‡]Earth Research Institute, University of California, Santa Barbara, CA 93106, United States

[§]University of California Center for Environmental Implications of Nanotechnology, University of California, Santa Barbara, CA 93106, United States

[⊥]University of California Center for Environmental Implications of Nanotechnology, California NanoSystems Institute, University of California, Los Angeles, CA 90095, United States

[‖]U.S. Environmental Protection Agency Office of Research and Development, National Exposure Research Laboratory, Athens, GA 30605, United States

[#]Department of Ecology, Evolution and Marine Biology, University of California, Santa Barbara, CA 93106, United States

[▽]Department of Chemistry, University of Texas at El Paso, El Paso, TX 79968, United States

## Abstract

The potential effects of carbonaceous nanomaterials (CNMs) on agricultural plants are of concern. However, little research has been performed using plants cultivated to maturity in soils contaminated with various CNMs at different concentrations. Here, we grew soybean for 39 days to seed production in soil amended with 0.1, 100, or 1000 mg $kg^{-1}$ of either multiwalled carbon nanotubes (MWCNTs), graphene nanoplatelets (GNPs), or carbon black (CB) and studied plant growth, nodulation, and dinitrogen (N2) fixation potential. Plants in all CNM treatments flowered earlier (producing 60% to 372% more flowers when reproduction started) than the unamended controls. The low MWCNT-treated plants were shorter (by 15%) with slower leaf cover expansion (by 26%) and less final leaf area (by 24%) than the controls. Nodulation and N2 fixation potential appeared negatively impacted by CNMs, with stronger effects at lower CNM concentrations. All CNM treatments reduced the whole-plant N2 fixation potential, with the highest reductions (by over 91%) in the low and medium CB and the low MWCNT treatments. CB and GNPs appeared to accumulate inside nodules as observed by transmission electron microscopy. CNM dispersal in aqueous soil extracts was studied to explain the inverse dose–response relationships, showing that CNMs at higher concentrations were more agglomerated (over 90% CNMs settled as agglomerates >3 μm after 12 h) and therefore proportionally less bioavailable. Overall, our findings suggest that

[*]Corresponding Author: holden@bren.ucsb.edu, 805-893-3195 (phone), 805-893-7612 (fax).

lower concentrations of CNMs in soils could be more impactful to leguminous N2 fixation, owing to greater CNM dispersal and therefore increased bioavailability at lower concentrations.

## TOC image

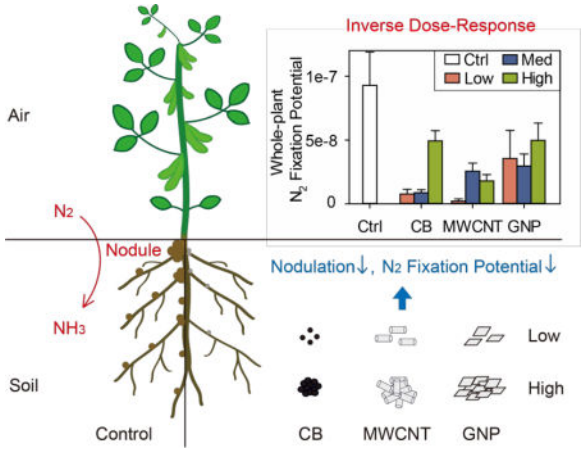


### Keywords

Carbonaceous nanomaterials; carbon nanotubes; graphene; bioavailability; agglomeration; soybean; dinitrogen fixation

The production and use of carbonaceous nanomaterials (CNMs), including carbon nanotubes (CNTs) and graphene, have rapidly increased.[1,2] Annual global production of CNTs has attained several thousand metric tons,[1] and graphene production is predicted to exceed 1000 metric tons annually by 2019.2 Once released into the environment, CNMs may accumulate in soils.[3,4] CNM-containing biosolids are applied to agricultural lands,[5] while CNM containing products are used both to remediate soils[6] and to fertilize and protect crops.[7] Given the potential for terrestrial plant and herbivore exposures, there is a need to understand hazards of CNMs to crop plants.[8–10]

Thus far, widely varying (including positive and negative) effects of CNMs on plants have been reported,[4,9,10] possibly owing to disparate study conditions including types and concentrations of CNMs, plant species and developmental stages, toxicity metrics, and exposure conditions. Hydroponic conditions have been used to study CNM effects at relatively high CNM concentrations (e.g., 500–2000 mg $L^{-1}$).[11,12] However, fewer studies simulate field conditions including using CNM concentration ranges that are predicted to occur in soils.[9,10,13] Many complex soil components (e.g., minerals and organic matter) can interact with CNMs and thereby affect CNM bioavailability.[6,9,14–16] Therefore, dose–response relationships for soil-grown plants cannot easily be inferred from hydroponic study results.[4] To assess CNM hazards to agricultural plants, more soil-based research using a wider range of CNM concentrations is needed.

In agricultural settings, plants not only root in the complex environment of soils, but plants also develop over time, including the maturation of root symbioses. Some CNM

phytotoxicity studies have emphasized acute toxicity on seed germination and seedling growth.[10] However, while such phytotoxicity assays offer the convenience of being standardized, they are performed over exposure periods that are too short to assess full agricultural impacts and are relatively insensitive for indicating nanotoxicity.[17] Additionally, plant–microbe rhizosphere interactions that regulate plant growth and productivity, biogeochemical cycling, and ecosystem functioning occur over the long time scales of agricultural production.[13,18] Such interactions could affect CNM-exposed plants under realistic conditions, since soil microbial communities[19] and microbe–plant interactions[20] appear sensitive to CNM exposures. Thus, researching CNM effects on plants in soil over long time periods usefully allows for assessing plants through their developmental, including reproductive, stages; life cycle studies in soil also allow for CNMs to interact with fast- or slow-growing rhizosphere microorganisms and symbioses.

In this study, we investigated the relative effects of multiwalled carbon nanotubes (MWCNTs), graphene nanoplatelets (GNPs), and carbon black (CB) on the growth, nodulation, and dinitrogen (N2) fixation potential of soybean grown to maturity in soil. Soybean (Glycine max) is an important food, animal feed, and biofuel crop species, accounting for 68% of global legume production.[21] Soybean has a critical role in the global nitrogen cycle by forming symbioses with N2 fixing bacteria in root nodules, fixing up to 16.4 million metric tons nitrogen annually in global agricultural systems (~77% of the total nitrogen fixed by leguminous crops).[21] N2 fixation by soybean decreases the need for fossil fuel-intensive synthetic nitrogenous fertilizers, whose extensive use leads to environmental impacts.[22] These impacts include nitrous oxide emissions, degraded ground and surface water quality, eutrophication, and harmful algal blooms.[21–23] Yet, soybean production and its associated N2 fixation apparatuses are potentially vulnerable to soil pollutants, including nanomaterials. For example, cerium dioxide (CeO2) nanoparticles inhibited soybean growth and yield, caused foliar stress and damage, and diminished N2 fixation potential.[24,25] However, less known are the potential effects of CNMs in soils on soybean growth and symbiotic N2 fixation.

Here, we evaluated three concentrations of each CNM (0.1, 100, and 1000 mg $kg^{-1}$ dry soil) to represent a range of possible environmental exposures[26] and explored how effects on soil-grown soybean varied with CNM type and concentration. Owing to our observations of plant effects, we performed separate studies of CNM concentration-dependent agglomeration in soil water extracts to determine how CNM concentration affected CNM dispersal and thus CNM bioavailability in soils. Our results demonstrate how the soil matrix can affect CNM bioavailability and thus dose-dependent effects of CNMs on soil-grown soybean and root nodule symbioses.

## RESULTS AND DISCUSSION

### CNM Characteristics

CB, MWCNTs, and GNPs were characterized by transmission electron microscopy (TEM), thermogravimetric analysis (TGA), and inductively coupled plasma optical emission spectroscopy (ICP-OES) before use. The three CNMs showed distinct morphologies and sizes (by TEM, Figures 1 and S1, Table S1). CB particles were spheroidal with an average

diameter of 36.6 ± 8.3 nm.[19] MWCNTs had an outer diameter of 18.8 ± 4.1 nm, which was slightly thinner than the manufacturer's reported value (Table S1). GNPs were two-dimensional flakes with an average size of 350 ± 320 nm (ranging from 80 to 1600 nm), which was much smaller than manufacturer's reported value (Table S1). The primary oxidation temperatures (an indicator of thermal stability, by TGA) for CB, MWCNTs, and GNPs differed and were approximately 620, 585, and 623 °C, respectively ($P < 0.05$; Table S1). Consistent with the high nanomaterial purities reported by the manufacturers (Table S1), the noncarbon impurities (by TGA) for CB, MWCNTs, and GNPs were 1.3%, 2.2%, and 1.0%, with an overall low metal content (by ICP-OES, that is, all lower than 0.1%, Table S2). An exception was that MWCNTs had a nickel (Ni) content of approximately 0.9%, which indicated the likely use of Ni catalyst for MWCNT synthesis.[27]

## CNMs Differentially Affect Soybean Aboveground Growth

In all treatments, plant stem length initially increased exponentially, but reached a maximum at approximately 22 d post-transplantation, which just followed the intermediate harvest (Figure 2A–C). Mostly, the CNMs had no significant effect on stem length (Figure 2A–C, Table S3). The exception was the low MWCNT treated plants, which were significantly shorter than the control plants at the final harvest ($P = 0.04$; Figure 2B, Table S3). Without including the control, the final stem length increased with MWCNT concentration, with plants in the low MWCNT treatment being significantly shorter than the medium ($P = 0.04$) and high ($P = 0.01$) MWCNT treatments (Table S3). Hereafter, we refer to such patterns (stronger CNM effects at lower concentrations) as "inverse dose–response relationships". The inverse dose–response relationship here between MWCNT concentration and the final stem length was well described by a power function ($r = 0.75$, $P = 0.002$; Figure S2A). Further, plants from the low MWCNT treatment showed slower leaf cover expansion ($P = 0.03$) and had reduced final total leaf area ($P = 0.02$) than the control plants (Figure 2E, Table S4). Both the leaf cover expansion rate constant and the final total leaf area increased with MWCNT concentration (Table S4). Without including the control, the inverse dose–response relationship was significant for the leaf cover expansion rate constant when modeled by a power function ($r = 0.56$, $P = 0.04$; Figure S2B) and for the final total leaf area when modeled by either a power ($r = 0.53$, $P = 0.05$; Figure S2C) or linear ($r = 0.55$, $P = 0.04$; Figure S2D) function. These trends suggest that the inhibitory effects of MWCNTs on soybean leaf development were reduced at the medium and high MWCNT concentrations (Table S4). There were no significant differences in either final leaf area or leaf cover expansion rate when comparing either the CB or GNP treatments with the control (Figure 2D, F, Table S4). Further, the CB, MWCNT, or GNP treatments did not affect trifoliate leaf count per plant (Figure S3A–C).

Previous hydroponic studies reported that MWCNTs (1000–2000 mg $L^{-1}$) reduced shoot lengths of red spinach, lettuce, and cucumber but not soybean,[11] while graphene (500–2000 mg $L^{-1}$) inhibited shoot lengths, leaf counts, and leaf areas of tomato, cabbage, and red spinach.[12] In our study, only the low MWCNT treatment significantly decreased soybean final stem length, leaf cover expansion rate constant, and final leaf area. In another study with soil-grown soybean, the low concentration (0.1 g $kg^{-1}$) of CeO2 nanoparticles most

strongly reduced soybean stem and leaf growth, compared to the medium (0.5 g $kg^{-1}$) and high (1 g $kg^{-1}$) concentrations.[24]

In contrast to the trends in vegetative growth, CNMs appeared to stimulate soybean reproductive development. Relative to the controls, plants in all CNM treatments had more flowers at the beginning of their reproductive stage (22 d post-transplantation, $P < 0.05$, except $P = 0.1$ and 0.08 for the high CB and low MWCNT treatments; Table 1, Figure S3D–F). The pod number per plant mostly appeared unaffected by CNM treatments, although plants in the high CB treatment had more total pods ($P = 0.03$) and all CB treatments had more mature pods (all $P < 0.05$), relative to the control (Figure S3G–I, Table S5). There was no significant difference in either the average seed count per pod or the pod size across all treatments (Table S5).

Prior studies have reported that CNMs could either inhibit or stimulate plant reproduction. For example, MWCNTs decreased the flower count of red clover[20] and delayed the flowering of rice plants;[28] in contrast, tomato produced twice as many flowers and fruits when watered with MWCNTs relative to unamended water.[29] These mixed effects could be attributed to the differences in exposure conditions, CNM characteristics and concentrations, and plant species. In our study, all CNM treated soybean produced more flowers, and the vegetative growth (e.g., stem length and leaf area) was significantly inhibited in the low MWCNT treatment. One mechanism that could explain the earlier flowering is that plants may accelerate their flowering when exposed to environmental stressors in order to maximize the chance of reproduction.[30] Thus, soybean may have responded to the low MWCNT inhibition by switching to reproductive growth and flowering early, at a cost to the final plant height and leaf area.

The aboveground tissue (stem, leaf, and pod) dry biomass and moisture content were measured at both harvests. From the intermediate to final harvest, each tissue type and the total aboveground dry biomass all increased substantially but did not differ significantly from the control or across CNM treatments (Figures S4A–C and S5A, Tables S6 and S7). The aboveground plant tissue moisture contents at both harvests were similar across treatments (Tables S8 and S9).

In summary, aboveground effects varied with CNM type and concentration. All CNMs accelerated soybean flowering, but only the low MWCNT treatment reduced plant height and final leaf area and slowed leaf canopy expansion.

## CNMs Inhibit Soybean Belowground Biomass and N2 Fixation Potential in an Inverse Dose-Dependent Manner

Soybean belowground (root and nodule) dry biomass and root nodule N2 fixation potential were measured at both harvests. Although dry root biomass did not vary across treatments at the intermediate harvest (Figure S4D, Table S6), plants in the low MWCNT treatment had lower dry root biomass than the controls at the final harvest ($P = 0.04$; Figure S4D, Table S7). Additionally, the final dry root biomass was significantly lower in the low MWCNT treatment than in the medium and high MWCNT treatments (both $P < 0.01$; Table S7). Without including the control, this inverse dose–response trend followed a power model (r =

0.79, P = 0.001; Figure S2E). The final dry root biomass was not affected by the CB and GNP treatments (Table S7). Root moisture content did not vary significantly across treatments (Tables S8 and S9).

The nodule count per plant is an indicator of the overall N2 fixation capacity.[24] At the intermediate harvest, plants from both the low and medium CB treatments as well as from the low MWCNT treatment formed fewer nodules than the controls (all $P < 0.05$; Figure 3A, Table S10). At the final harvest, the nodule count was significantly lower in the medium CB and low MWCNT treatments than in the control (both $P < 0.05$; Figure 3A, Table S11). Further, the nodule count increased from the low MWCNT treatment to the medium (intermediate P = 0.009, final P = 0.04) and high (intermediate P = 0.02, final P = 0.04) MWCNT treatments, although the medium and high treatments did not differ from each other (Tables S10 and S11). At the final harvest, the apparent inverse dose–response trend was significant when fitted by a power model (r = 0.74, P = 0.002; Figure S6A). In the low GNP treatment, the nodule count decreased from the intermediate to the final harvest, when it appeared to be lower than the control level (P = 0.07; Figure 3A, Tables S10 and S11). This would result if some of the early nodules decayed and failed to mature due to GNP exposure. Within the GNP treatments, there was an apparent inverse dose–response relationship: the final nodule count increased linearly with GNP concentration (r = 0.69, P = 0.004; Figure S6B).

In the period between the intermediate and final harvests (when soybean initiated reproductive development), root nodule dry biomass per plant increased substantially in all treatments, but the average 9.6-fold increase significantly varied across treatments (Figure 3B, Tables S6 and S7). At the intermediate harvest, the dry nodule biomass was reduced (compared to the control) for both the low and medium CB treatments as well as for the low MWCNT treatment (all $P < 0.05$; Figure 3B, Table S6). The reduction in nodule biomass was more extensive at the final harvest, since all MWCNT and most CB treatments as well as the low GNP treatment resulted in less dry nodule biomass than the control (all $P < 0.01$, except P = 0.06 for the high CB treatment; Figure 3B, Table S7). At the intermediate harvest, the dry nodule biomass in the medium CB treatment was similar to that in the low CB treatment, but significantly lower than in the high CB treatment (P = 0.05; Figure 3B, Table S6); at the final harvest, both the low and medium CB treatments had less dry nodule biomass than the high CB treatment (both $P < 0.05$; Figure 3B, Table S7). Within the MWCNT treatments, the final dry nodule biomass was significantly less in the low MWCNT treatment than in the medium and high MWCNT treatments (both $P < 0.01$; Figure 3B, Table S7). Also, there was an inverse dose–response relationship within the GNP treatments without including the control: the final dry nodule biomass increased linearly (toward control levels) with GNP concentration (r = 0.74, P = 0.002; Figure S6C).

Dividing total dry nodule biomass by nodule count for each individual plant yielded the average dry biomass per nodule (Figure 3C, Tables S10 and S11). The dry biomass per nodule is indicative of how many bacteroids (the symbiotic form of N2 fixing bacteria) are contained in the nodule central tissue, since the thickness (and hence mass) of nodule cortex tissue is relatively constant regardless of nodule size.[31] At the intermediate harvest, plants from the medium CB and low MWCNT treatments formed nodules with lower average dry

biomass than the controls (both $P < 0.05$; Figure 3C, Table S10). At the final harvest, for the low and medium CB treatments and for all MWCNT treatments, the dry biomass per nodule was approximately half or less than half of the control level (all $P < 0.001$; Figure 3C, Table S11). Within the CB treatments, the final dry biomass per nodule was lower in the low ($P = 0.004$) and medium ($P = 0.003$) CB treatments as compared to the high CB treatment (Table S11). The final dry biomass per nodule was significantly lower in the low MWCNT treatment than in the medium and high MWCNT treatments (both $P < 0.001$; Table S11). Additionally, the dry biomass per nodule at the intermediate harvest appeared to increase with GNP concentration toward control levels; without including the control, this inverse dose–response trend was significant when modeled by a power function ($r = 0.71$, $P = 0.03$; Figure S6D). The decrease in the dry biomass per nodule arose from nodule sizes decreasing, since nodule moisture contents were mostly invariant across treatments (Tables S8 and S9). In previous hydroponic studies, nanoscale zinc oxide (ZnO, 100–1000 mg $L^{-1}$)[32] and titanium dioxide (TiO2, 250–750 mg $L^{-1}$)[33] were found to reduce the nodule size in the symbioses between garden pea and Rhizobium leguminosarum bv. viciae 3841.

It may be noteworthy that, at both harvests, the low MWCNT treatment had the lowest total dry nodule biomass, nodule count, and dry biomass per nodule (Tables S6, S7, S10, and S11). These results were unlikely to have arisen from the Ni impurity (0.9%, Table S2) of MWCNTs. Assuming that all of the Ni contained in the low (0.1 mg $kg^{-1}$) MWCNT treatment was bioavailable, the Ni concentration would be only 0.0009 mg $kg^{-1}$. This concentration is far below the Ni dose reported to inhibit soybean nodulation (1 ppm).[34]

Measured as the specific activity of nitrogenase (the universal enzyme for biological N2 fixation) by the acetylene reduction assay, the N2 fixation potential is expressed as ethylene production rate normalized to dry nodule biomass. CNMs reduced soybean N2 fixation potential differentially according to CNM dose, type, and harvest stage (Figure 3D, Tables S10 and S11). At the intermediate harvest, significantly different from the controls, plants from the low MWCNT treatment had no measurable N2 fixation potential ($P = 0.008$; Figure 3D, Table S10). At the final harvest, N2 fixation potentials were significantly lower than the control levels for both the low and medium CB treatments as well as for the low MWCNT treatment (all $P < 0.05$; Figure 3D, Table S11). Within the CB treatments without including the control, the final N2 fixation potential increased linearly with CB concentration ($r = 0.77$, $P = 0.001$; Figure S6E), indicating that the CB inhibition of N2 fixation potential was mitigated at higher CB concentrations.

The whole-plant N2 fixation potential was calculated as the product of the dry nodule biomass per plant and the N2 fixation potential normalized to dry nodule biomass.[35,36] The result represents both the total amount of nitrogenase that has been synthesized and the specific nitrogenase activity and therefore provides an overall assessment of N2 fixation capacity on a whole plant basis. At the intermediate harvest, across all CNM treatments except for the medium GNP treatment, the wholeplant N2 fixation potential appeared diminished relative to the control by 30% or more (Figure S7A, Table S10). The inhibition appeared to be 90% or more for the low and medium CB treatments (both $P = 0.09$) and was 100% for the low MWCNT treatment ($P = 0.02$; Figure S7A). At the final harvest, all CNM treatments appeared to reduce the whole-plant N2 fixation potential by 46% or more relative

to the control (Figure S7B, Table S11). Whole-plant N2 fixation potentials in both the low and medium CB treatments and in the low MWCNT treatment were less than 10% of the control level (all $P = 0.001$); in the medium and high MWCNT treatments, values were less than 28% of the control level (both $P < 0.01$). Within the CB treatments, without including the control, the final whole-plant N2 fixation potential appeared to increase linearly with CB concentration ($r = 0.90$, $P < 0.001$; Figure S6F), although the differences between the low and medium CB concentrations did not appear to be significant (Table S11). Kapustka and Wilson[36] previously reported a compensatory relationship between the specific nitrogenase activity and dry nodule biomass per plant: the reduction in soybean N2 fixation potential was offset by an increase in total dry nodule biomass, resulting in a higher final yield. However, we did not observe such a compensatory mechanism here as both the final total dry nodule biomass and the final N2 fixation potential appeared reduced in most CNM treatments relative to the control (Figure 3B, D). This compounded each effect, resulting in relatively greater diminishment in the final whole-plant N2 fixation potential (Figure S7B).

TEM analyses were performed at the final harvest to examine the potential ultrastructural changes and CNM accumulation inside soybean root nodules. The low CNM concentration treatments were prioritized, since they appeared more impactful than higher CNM concentration treatments. For control nodules (Figure 4A, B), infected nodule cells were densely packed with symbiosomes, inside which bacteroids were present and surrounded by the symbiosome membrane.[31] Electron-translucent granules inside bacteroids were likely poly(β-hydroxybutyrate) (PHB, Figure 4A)[31] that had accumulated as carbon reserves during active photosynthesis, for fueling N2 fixation under low carbon availability periods.[37] In the low CB (Figure 4D) and low MWCNT (Figure 4E, F) treatments, nodules appeared comparatively empty and had atypical large vacuoles.[38] The bacteroid density inside nodules, determined by quantitative analysis of nodule TEM images (Supporting Information), was significantly lower in the low CB and low MWCNT treatments than in the control (both $P < 0.05$; Table S12). This lack of bacteroids corroborates the findings herein that nodules in the low CB and low MWCNT treatments had significantly lower final dry biomass per nodule and final N2 fixation potential than the controls (all $P < 0.01$; Figure 3C, D, Table S11). Densely packed bacteroids were evident in the low GNP treatment (Figure 4H). The bacteroid width measured from nodule TEM images (Supporting Information) of all three low CNM treatments differed significantly from that of the control (all $P < 0.001$; Table S12). Further, black particles with sizes comparable to that of dry CB powder (Figures 1A and S1A) were observed in both the symbiosome (associated with a bacteroid) and nodule cell cytoplasm (Figure 4C), indicating uptake of CB into nodules. The accumulation was also apparent for GNPs (Figure 4G, H): both single and aggregated structures with morphologies similar to that of GNP dry powder (Figures 1C and S1C) were observed inside nodules. No MWCNTs were observed in the nodule TEM specimens. The CNMs accumulated inside nodules were not likely to interfere with the N2 fixation potential measurement (Supporting Information). Additionally, in all three CNM treatments, putative starch granules, indicative of low N2 fixation activity,[39] appeared inside nodule cells (Figure 4D, F, G).

Where they occurred, reductions in nodule count, dry nodule biomass, and N2 fixation potential in the CNM treatments would indicate that CNMs had negatively impacted many

steps during root nodule development.[38] The possible explanations include toxicity to either the soybean plant or N2 fixing bacteria, or both. The low MWCNT treatment stunted soybean stem and leaf growth, and reduced the final dry root biomass. Plants from this treatment also formed fewer nodules with the least dry biomass and the lowest N2 fixation potential. As such, toxicity to the plant could have inhibited nodulation and N2 fixation potential in the low MWCNT treatment. Previously, CeO2 nanoparticles caused soybean leaf oxidative stress and damage; these effects corresponded with root nodule N2 fixation potential diminishment, with the explanation that the plant preferentially invested energy aboveground rather than to nodules belowground.[25] Phytotoxicity was reported to reduce nodule count in the Medicago truncatula–Sinorhizobium meliloti symbioses exposed to nanoparticle-containing (Ag, ZnO, and TiO2) biosolids; multiple nodulation-related genes of M. truncatula were downregulated in the nanoparticle treatment relative to those in either the control or the treatment with bulk/ionic forms of the metals.[40]

Alternatively, Bradyrhizobium japonicum (the N2 fixing bacterium that colonizes soybean) could have been negatively affected by CNMs in the soil.[32,33] The toxicity might manifest as killing, thus lowering the abundance of infecting bacteria. There could have also been altered bacterial metabolism with impeded signal communication with soybean plant roots. CNMs might have damaged bacterial cell membranes, hence rendering bacteria incapable of attaching to root hairs to begin the infection process.[33] Some defective bacteria might enter an infection thread but would not proliferate normally; they might also become trapped, thus disabling the infection thread.[33] Empty nodules could form if stressed B. japonicum did not penetrate nodule cells to form symbiosomes and differentiate into bacteroids, even though early nodule establishment was successful. Additionally, CNMs could have sorbed onto B. japonicum, thus allowing for CNM-coated bacteria to become engulfed in the infection thread. In such cases, B. japonicum might have carried CNMs into nodule cells, during which B. japonicum might have been continuously exposed to CNMs. The accumulation of starch granules in CNM treated nodules suggests that bacteroids could be defective, that is, either not fully differentiated with normal N2 fixation capability or having defective metabolism.[39] As a result of the low N2 fixation efficiency, soybean plants may have responded by reducing carbon supply to these nodules and further suppressing N2 fixation.[41]

Besides possibly being transported by B. japonicum, CNMs could also have been taken up by nodule cells directly. The pore size of plant cell wall is commonly estimated to be 5–20 nm, and hence nanomaterials larger than 20 nm would be excluded.[14] However, new pores with larger diameters might form on plants to facilitate nanomaterial uptake.[14] It has been reported that the pore size can be as large as 50 nm, as evidenced by the observation of gold nanoparticles (~50 nm) inside tobacco plants.[42] In the present study, CB nanoparticles had a size of 36.6 ± 8.3 nm[19] (Figures 1A and S1A, Table S1), which suggests CB could cross plant cell walls. MWCNTs could also be taken up when oriented perpendicularly to the cell surface since the outer diameter was 18.8 ± 4.1 nm (Figures 1B and S1B, Table S1). Previously, both individual and aggregated MWCNTs were found (by two-photon excitation microscopy) to be piercing wheat roots and entering the root cell cytoplasm in a hydroponic study,[43] while direct MWCNT uptake from soil into a root cell of red clover was observed by TEM.15 The apparent accumulation of GNPs inside nodules is also interesting, as GNPs have a thickness of 8–12 nm but a larger diameter (350 ± 320 nm; Figures 1C and S1C,

Table S1). It could be possible that GNPs might have folded into sheets of smaller diameters, or there might be additional internalization pathways for GNPs. In a previous hydroponic study, graphene oxide (1 mg $L^{-1}$, with a size of 192 ± 24 nm) was demonstrated to accumulate inside root cells of Arabidopsis plants.[44]

In summary, CB, MWCNTs, and GNPs negatively affected soybean nodulation (i.e., nodule count, nodule dry biomass, or dry biomass per nodule) and N2 fixation potential, particularly at lower concentrations. Nanomaterials appeared to accumulate inside nodules in the low CB and low GNP treatments, suggesting direct CNM interference with N2 fixing symbioses.

## CNMs Agglomerate at Higher Concentrations in Soil

To test the role of CNM agglomeration in the observed inverse dose–response relationships, we studied CNM agglomeration and sedimentation in aqueous soil extracts (soil characteristics detailed in Table S13). We used two CNM concentrations (10 and 300 mg $L^{-1}$, Supporting Information) for CB, MWCNTs, and GNPs, to investigate the effect of CNM concentration on CNM colloidal stability, and thus on CNM bioavailability. At the higher CNM concentration (300 mg $L^{-1}$), all CNMs agglomerated rapidly after CNMs were mixed into the soil extract, with the hydrodynamic diameter increasing to several micrometers; less than 22% of the nanomaterials remained suspended after 2 h (Figure 5). After 12 h, more than 90% of CNMs at 300 mg $L^{-1}$ settled out as large agglomerates (Figures 5, S8 and S9). At the lower CNM concentration (10 mg $L^{-1}$), negligible agglomeration and sedimentation were observed for all CNMs in the soil extract in the first 2 h, although over the following 56 days there was gradual formation of smaller aggregates (<400 nm) that slowly settled out (Figures 5, S8 and S9).

Across CNMs, at the 10 mg $L^{-1}$ concentration, CB was significantly more stable in the soil extract than the other two CNMs, according to normalized nanomaterial suspension absorbances and hydrodynamic diameters (Figures 5, S8 and S9). After 7 d, CB (10 mg $L^{-1}$) was more well dispersed, with a smaller average hydrodynamic diameter (267 ± 5 nm) as compared to MWCNTs (10 mg $L^{-1}$, 387 ± 3 nm) and GNPs (10 mg $L^{-1}$, 289 ± 4 nm) in the soil extract suspension ($P = 0.000$; Figures 5, S8 and S9). This was also supported by the zeta (ζ) potential and electrophoretic mobility (EPM) measurements, in which 10 mg $L^{-1}$ CB had a more negative ζ potential and EPM than either the 10 mg $L^{-1}$ MWCNTs or the 10 mg $L^{-1}$ GNPs (all $P < 0.05$; Table S14).

Environmental scanning electron microscopy (ESEM) was performed to observe the agglomerate morphologies of 10 and 300 mg $L^{-1}$ CNMs in the soil extract upon deposition onto clean quartz sand (Figure 6). At the lower concentration (10 mg $L^{-1}$), CB, MWCNTs, and GNPs appeared dispersed, with their surfaces apparently covered by a thin layer of organic matter from the soil extract (Figure 6A, C, E). By contrast, at the higher CNM concentration (300 mg $L^{-1}$), large agglomerates, with sizes of several micrometers, were observed (Figure 6B, D, F). Specifically, CB formed loose appearing agglomerates composed of smaller aggregates, and MWCNTs were entangled together resulting in porous agglomerates, but GNPs appeared to stack together and were embedded in polymeric material, forming more compact agglomerates.

The magnitude of CNM effects on soil microorganisms and plants depends partly on CNM bioavailability, which in turn is affected by CNM dispersal in soil pore water.[6,9,14,15] Soil pore water is often rich in dissolved organic matter,[16] which can improve CNM dispersal in the aqueous phase.[45] However, the cationic content of soil pore water would shrink the electrical double layer and thus diminish electrostatic repulsion. As van der Waals forces increase relative to repulsive forces, CNMs agglomerate.[16] Naturally occurring colloids in soil pore water could also affect CNM dispersal by heteroaggregation.[16] To explain the observed inverse dose–response relationships (Figures S2 and S6), we hypothesized that, as CNM concentration increased, nanomaterials agglomerated into larger structures with relatively low bioavailability in soil. Such agglomeration-induced decreases in CNM bioavailability led to decreased CNM effects on plants and root symbioses at higher CNM concentrations.

Through the agglomeration study, we confirmed that CNM agglomeration increased with increasing CNM concentration in soil water extracts. The differing CNM colloidal stability across the two CNM concentrations may be attributed to soil physicochemical properties (Table S13), in particular, ionic strength.[46] In deionized water (low ionic strength), electrostatic repulsion dominated between CNMs with diminished van der Waals attraction, resulting in relatively stable CNM suspensions.[46] For each CNM type, CNM hydrodynamic diameters in deionized water immediately following sonication were similar across CNM concentrations, averaging 204 ± 8 nm (CB), 333 ± 27 nm (MWCNTs), and 242 ± 9 nm (GNPs) across 10 and 300 mg $L^{-1}$ (Table S15). However, in the soil extract (higher ionic strength), when the van der Waals forces were stronger than repulsive force due to electrical double layer shrinking, CNMs agglomerated; the degree of agglomeration increased with CNM concentration.[46] Additionally, at the higher CNM concentration (300 mg $L^{-1}$), the collisions between particles increased,[16] and the effect of dissolved organic matter on improving CNM dispersal was decreased.[45] Collectively, the effect of CNM concentration on CNM agglomeration was exacerbated in the soil extract.

It is worth noting that CNM agglomeration dynamics could be more complex in situ in soils, particularly in the rhizosphere due to root uptake, rhizospheric exudation, and microbial processes.[13,16] For example, plant roots can release many lowmolecular-mass compounds (including amino acids, organic acids, and sugars) that can affect soil pH and CNM agglomeration.[16] Root exudation may also be altered after nanomaterial exposure.[47] In addition, adsorption of nanomaterials to bacterial cell surfaces has been reported to disperse nanomaterial agglomerates.[48] Such processes and other soil characteristics (e.g., redox potential, texture, organic matter, and clay minerals) could cause temporal variations in CNM behavior within the natural soil environment, including differentially over the course of plant growth.

The results of the CNM concentration-dependent agglomeration in aqueous soil extracts qualitatively explained the observed inverse dose–response trends, which deviate from typical sigmoidal dose–response relationships reported for toxicants that dissolve in soil water[34] (Figure 7), but quantitative tests are not possible because of the complex soil characteristics and dynamic processes described above. In this study, with nondissolving but agglomerating CNMs, small amounts of CNMs in moist soil did not agglomerate but rather

remained suspended in soil water where they were more bioavailable and impactful to soil microbes and plant roots. With larger amounts of CNMs in moist soil, large agglomerates formed, which led to a sharp decrease in their bioavailability and observed impacts (Figure 7). Although the inverse dose–response patterns were mostly shared across CNMs, the relationships were linear for CB (Figures 7 and S6) and fit a power function for MWCNTs (Figures S2 and S6). Differences in agglomeration and possibly differing toxicity mechanisms (albeit not studied herein) could explain the differing model fits.

Our results demonstrate that not only the mass concentration and primary particle size but also the level of agglomeration may play critical roles in determining CNM effects on plants and their root symbioses in soils. In prior microbial toxicity and hydroponic phytotoxicity studies, it was recognized that nanomaterial effects would increase as nanomaterial size decreases but would decrease as nanomaterials agglomerate. For instance, antimicrobial activity was found to be higher for smaller versus larger graphene oxide sheets,[49] while debundled, short, and dispersed MWCNTs were demonstrated to have relatively higher bacterial cytotoxicity due to enhanced MWCNT–cell contact.[50] Depicted as “nano darts”, individually dispersed single-walled carbon nanotubes (SWCNTs) were reported to induce more bacterial death than SWCNT aggregates, as dispersed SWCNTs directly damaged bacterial cell membranes.[51] In hydroponic studies, dispersed MWCNTs were found to have stronger effects on tomato plants than MWCNT agglomerates.[52] Even when comparing among agglomerates, small MWCNT agglomerates exerted stronger impacts to Arabidopsis T87 cells than large agglomerates.[53]

Still, the dose–response relationship for unstudied low concentrations, which are, across the herein unstudied range of 0 to 0.1 mg $kg^{-1}$, is uncertain. It is possible that the whole-plant N2 fixation potential decreased continuously with CB concentration until 0.1 mg $kg^{-1}$ (Figure 7, “Scenario 1”). Alternatively, there could be a threshold concentration somewhere between 0 and 0.1 mg $kg^{-1}$, possibly close to the lowest studied dose (0.1 mg $kg^{-1}$), above which the inhibition of the whole-plant N2 fixation potential occurred but below which it did not (Figure 7, “Scenario 2”). There is uncertainty in such untested low concentration regimes. Such uncertainty reinforces the challenges in extrapolating toxicological results from studies using only high nanomaterial concentrations to low concentration exposure scenarios, owing to influential effects of nanomaterial physicochemical structuring.[54]

## CONCLUSIONS

In summary, MWCNTs, GNPs, and CB significantly affected soil-cultivated soybean, particularly the symbioses with N2 fixing bacteria. We observed inverse dose–response relationships: lower concentrations of CNMs were relatively more impactful to soybean growth, root nodulation, and N2 fixation potential. Direct evidence from studies of CNM agglomeration in aqueous soil extracts suggested that the inverse dose–response relationships were caused by reduced CNM bioavailability at higher CNM concentrations, due to more extensive CNM agglomeration. Our results show the importance of including low CNM concentrations close to predicted exposure scenarios and characterizing nanomaterial physicochemical characteristics related to bioavailability in soils during phytotoxicity assessment. The significant treatment effects observed here suggest that

symbiotic N2 fixation can potentially be used as a sensitive metric for evaluating nanomaterial risks in the terrestrial environment compared to other standard phytotoxicity assays, which were suggested as relatively insensitive. Overall, our results indicate that the potential accumulation of CNMs in soils could inhibit symbiotic N2 fixation in soybean, which is an agriculturally important leguminous crop plant. This research contributes to a better understanding of the potential implications of carbonaceous nanomaterials in agricultural systems.

## METHODS

### Carbonaceous Nanomaterials

We chose multiwalled carbon nanotubes (MWCNTs) and graphene nanoplatelets (GNPs) as two representative engineered CNMs, with industrial carbon black (CB) for comparison. CB has been commercialized for decades in the rubber and pigment manufacturing industries,[2] with annual production of over 10 million metric tons.[26] CB has been deemed persistent in the environment but with a low potential for bioaccumulation and toxicity.[55] However, there is evidence that CB may have similar or higher toxic effects on soil bacterial communities and amphipods compared with other CNMs.[19,56] Therefore, assessing whether CB affects soybean and N2 fixing symbioses and comparing how the effects differ from those of MWCNTs and GNPs are important from an environmental regulatory standpoint.

MWCNTs and GNPs were purchased from Cheap Tubes Inc. (Grafton, VT); carbon black (CB, Printex 30) was purchased from Dorsett & Jackson Inc. (Los Angeles, CA). Besides the manufacturer reported properties (including purity, size, and specific surface area, Table S1), CNMs were characterized by transmission electron microscopy (TEM; JEOL 1200 EX, Peabody, MA), thermogravimetric analysis (TGA; TA Discovery Thermogravimetric Analyzer, New Castle, DE), and inductively coupled plasma optical emission spectroscopy (ICP-OES; Thermo iCAP 6300, Waltham, MA) for material morphology, thermal stability, overall purity, and metal composition, following previously reported methods.[19,57] The CNMs were used as received without further purification.

### Soil

Sandy-clay-loam agricultural soil was collected from the University of California Sedgwick Reserve, CA (34°40′32″N, 120°2′27″W). After transport to the laboratory, the soil was sieved (4 mm) to remove rocks, roots and fresh litter, then stored (4 °C). Soil salinity, nutrient content, and other physicochemical properties, including texture, pH, water saturation (%), cation exchange capacity, soluble salts, organic matter, total nutrients (C, Cu, Fe, Mn, N, Zn), extractable nutrients (B, Ca, Cl, Cu, Fe, Mg, Mn, Na, P, Zn, $HCO3^{-}$, $CO3^{2-}$, $NH4^{+}$, $NO3^{-}$), and exchangeable nutrients (Ca, K, Mg, Na), were characterized at the University of California at Davis Analytical Laboratory (http://anlab.ucdavis.edu/), according to standard methods (Table S13).

### Nanomaterial Amendment to Soil

Three concentrations of MWCNTs, GNPs, and CB (0.1, 100, and 1000 mg $kg^{-1}$ dry soil) were evaluated in this study. A sequential 10-fold dilution method accompanied by

mechanical mixing was used to prepare homogenized soil and CNM mixtures as reported previously.[24] The mixing was performed using a hand-held kitchen mixer, from the low to the high CNM concentration treatments, with the mixer cleaned between different CNMs to avoid contamination. The cleaning procedure followed guidelines recommended by the National Institute for Occupational Safety and Health (NIOSH) for cleaning surfaces contaminated with carbon nanotubes.[58] CNM dry powder was weighed and amended directly into soil in concentrations of 0.01, 10, and 100 g $kg^{-1}$ (dry soil basis). Each mixture was blended thoroughly using the mixer for at least 10 min. These CNM–soil stocks were then diluted ten times by the addition of unamended soil and mixing by the mixer similarly as above, resulting in concentrations of 0.001, 1, and 10 g $kg^{-1}$. The dilution and mixing were repeated again to achieve the final CNM working concentrations of 0.1, 100, and 1000 mg $kg^{-1}$. The CNM–soil mixtures were stored (enclosed, room temperature) prior to planting.

### Bacterial Inoculum and Soybean Planting

Bradyrhizobium japonicum USDA 110 (U.S. Department of Agriculture, Washington, DC) was initially streaked from frozen stock (maintained at −80 °C in 70% Luria–Bertani broth plus 30% (v/v) glycerol) onto solid modified arabinose gluconate (MAG) medium[24] with 1.8% (w/v) agar in a Petri dish, then cultivated (5 d, 30 °C) in the dark. Following incubation, several discrete colonies were dispersed into 4 mL of liquid MAG medium. An aliquot (50 μL) was inoculated into a 500 mL glass flask containing 100 mL of liquid MAG medium and incubated (30 °C, shaking at 200 rpm) in the dark for 5 d until stationary growth phase. Aliquots of the culture were dispensed into centrifuge tubes and centrifuged (10 000 × g, 10 min), and the supernatant was discarded. Cell pellets were resuspended in a 1 M MgSO4 solution to an optical density at 600 nm (OD600) of 1.0 to serve as the inoculum during seed planting.

Soybean seeds (Glycine max, Midori Giant variety, lot no. WA15060001) were purchased from Park Seed Co. (Hodges, SC). Seeds were inoculated with B. japonicum following the method of Priester et al.[24] Specifically, seeds were soaked in the B. japonicum inoculum for 10 min and deposited into rehydrated peat-filled seed starter pellets (Park Seed Co., Hodges, SC) at 1/4-in. depth using forceps. An aliquot (100 μL) of the B. japonicum inoculum was dispensed into the pellet holes over the planted seed; the seed plus additional inoculum were then covered with a thin layer of the peat pellet substrate. The pellets were watered daily and incubated on a heating mat (23 °C).

### Soybean Seedling Transplantation into Soil Amended with Carbonaceous Nanomaterials

Each planting pot was comprised of a 3 qt (2.84 L) high density polyethylene (HDPE) container with bottom perforations, which was lined with polyethylene WeedBlock fabric (Easy Gardener Products, Waco, TX) at the bottom, and overlain by 400 g of washed gravel (Quikrete, Atlanta, GA) to allow water drainage. A polyethylene bag punched with 40 evenly spaced 5 mm holes was placed over the gravel, and 2.3 kg of soil (dry basis, for each treatment) was weighed into each bag. Perforation of the bags allowed for water drainage, thereby preventing root rot within the soil-filled bags. Overall, there were 10 treatments, including three concentrations (0.1, 100, and 1000 mg $kg^{-1}$) for each of CB, MWCNTs, and

GNPs, plus a control soil without nanomaterial amendment. There were eight replicate pots per treatment.

Ten days after seed sowing, 80 VC stage (with unrolled unifoliate leaves)[59] seedlings were transplanted into potted soils. Prior to transplanting, the outside mesh of the starter pellets was removed carefully to minimally disturb the seedling roots. A central planting hole was formed in the soil, into which B. japonicum inoculum (5 mL, prepared as above) was dispensed. One seedling was inserted into the hole, and another aliquot (5 mL) of B. japonicum inoculum was dispensed onto the surface. Both inoculation steps were deemed necessary for adequate contact between B. japonicum and the soybean roots and thus effective inoculation. The filled transplanting hole was covered by a thin layer of soil, and the potted soil surface covered by a layer of WeedBlock fabric to minimize soil surface crusting and weed growth. A wooden support stake was inserted against the inside wall of each pot for later plant support by tying, as needed.

## Plant Growth Conditions

After transplanting, the plants were grown for another 39 d to the R6 stage (with seed-filled pods)[59] in the Schuyler Greenhouse at the University of California at Santa Barbara. The greenhouse climate was controlled using VersiSTEP automation (Wadsworth Control Systems Inc., Arvada, CO) under full sunlight. The indoor air temperature ranged from 15 to 34 °C, and the indoor photosynthetically active radiation (PAR) fluctuated between 21 and 930 μmol $m^{-2}$ $s^{-1}$ from nighttime to daytime. Soil moisture sensors (model 5TE, Decagon, Pullman, WA) were inserted to a depth of 13 cm into the soil of seven pots (control and 100 and 1000 mg $kg^{-1}$ of CB, MWCNTs, and GNPs) to monitor soil volumetric water content, electrical conductivity, and temperature. Data were recorded at least twice daily using a ProCheck data display (Decagon, Pullman, WA). Pots were watered to retain an average soil volumetric water content of 0.25 $m^3$ $m^{-3}$ (Figure S10).

## Plant Growth Measurements

Immediately following transplanting, plant growth was assessed twice weekly by measuring stem length, the number of leaves, flowers, and pods, and developmental (vegetative and reproductive) stages according to Pedersen[59] and Priester et al.[24] Aerial photos were acquired weekly directly above each plant and analyzed using Adobe Photoshop software to quantify the leaf cover, following the method of Priester et al.[24]

## Harvests

Midori Giant is a determinate soybean variety, which stops vegetative growth soon after flowering initiates.[59] Also, N2 fixation will accelerate when plants initiate pod development.[35,59] Therefore, plants were harvested at each of two stages: intermediate (before reproduction, defined as flowering) or final (full seed production, before senescence), aimed at capturing CNM effects on plant vegetative growth with early nodule formation, and then reproductive development with highest N2 fixation potential. Three replicate plants from each of the ten treatments were sacrificed at the intermediate harvest (20 to 21 d post transplantation), and five replicates were sacrificed at the final harvest (39 to 41 d post-transplantation), when plants reached stage R6 (seed filled pods).[59] At harvest, plants were

separated, aboveground from belowground, by cutting the stem at the soil surface using a single edge razor blade. The aboveground part was further divided into stem, leaves, and pods (if present). Leaves and pods were counted and arranged according to their sizes, then photographed. Total leaf area and pod size were further quantified by analyzing the images using Adobe Photoshop software.[24] Subsamples of fresh leaves and pods were weighed and then stored for future analyses. The remaining tissues were transferred to separate paper bags, then weighed before and after drying (60 °C, 3 d) to determine wet and dry biomass plus gravimetric moisture content.

The belowground plant parts were removed from the pot within the polyethylene bag surround. The soil in the bag was gently loosened from around the roots and nodules using a metal Scoopula (Fisher Scientific, Waltham, MA), while minimizing root system disturbance. The relatively intact belowground parts, including roots and nodules, were rinsed in deionized water thoroughly to remove remaining attached soil, then air-dried. The nodules were carefully excised from the roots using a single edge razor blade and forceps as reported previously.[24] Nodules were counted; subsamples were weighed and refrigerated (4 °C) for later TEM analysis. The remaining nodules were weighed and then analyzed immediately for N2 fixation potential. Roots were dried and massed as above, to determine gravimetric moisture content and dry biomass. After N2 fixation potential measurements, nodules were also similarly dried and massed. After acquiring dry masses, all dried plant parts were archived for future analyses. Subsamples of soil from each pot were collected and stored (−80 °C) for future analyses.

### Root Nodule Dinitrogen Fixation Potential

The N2 fixation potentials of root nodules were measured as nitrogenase activity by the acetylene reduction assay, according to standard methods with some modifications.[60] Pure acetylene (C2H2) gas was generated by the reaction of calcium carbide (CaC2, 12 g) and deionized water (200 mL) in a 1 L Erlenmeyer flask, with C2H2 collected into a 1 L Tedlar bag (Supelco Inc., Bellefonte, PA). Intact nodules that were freshly excised from cleaned plant roots were placed into a 60 mL syringe with a LuerLok Tip (BD, Franklin Lakes, NJ) and incubated with 10% C2H2 (6 mL of pure C2H2 plus 54 mL of air). At 0, 15, 30, 45, and 60 min, 10 mL of the gas sample in the syringe was injected into an SRI 8610C gas chromatograph (GC; SRI Instruments, Torrance, CA) with a sample loop (0.25 mL) to measure the C2H2 reduction to ethylene (C2H4) over time. The GC was equipped with a flame ionization detector (FID) and a 3 ft × 1/8 in. silica gel packed column. Helium (He) was used as the carrier gas at a pressure of 15 psi (~21 mL $min^{-1}$). Hydrogen (H2) gas and air were supplied for FID combustion at 25 and 250 mL $min^{-1}$, respectively. The oven temperature was held constant (145 °C). The C2H4 peak area and retention time (~0.78 min) were recorded using PeakSimple Chromatography Software (SRI Instruments, Torrance, CA). Chemically pure C2H4 gas (Matheson Tri-Gas Inc., Basking Ridge, NJ) was diluted by air and measured to establish a C2H4 standard curve (C2H4 concentrations 0, 0.4‰, 0.8‰, 1.6‰, 3.1‰, and 6.3‰). The C2H4 peak area values were converted to C2H4 concentrations against the standard curve and further to moles of C2H4 using the ideal gas law assuming ambient temperature and pressure. For each analysis, the moles of C2H4 produced were plotted over time, and the relationship was evaluated for linearity, then fitted

by a linear regression model to calculate the C2H4 production rate. The N2 fixation potential (mol C2H4 $min^{-1}$ $g^{-1}$) was calculated as the C2H4 production rate normalized to the assayed dry nodule biomass. The whole-plant N2 fixation potential (mol C2H4 $min^{-1}$ $plant^{-1}$) was calculated by multiplying the total dry nodule biomass of each plant and the N2 fixation potential, which had been normalized to dry nodule biomass.

### Transmission Electron Microscopy of Root Nodules

Cleaned root nodules were fixed in phosphate buffered 2% glutaraldehyde, postfixed with 1% osmium tetroxide, dehydrated in a graded series of ethanol, and embedded in Spurr resin (Ted Pella Inc., Redding, CA). Ultrathin cross sections (70 nm thickness) were obtained using a Leica Ultramicrotome UC7 (Leica Microsystems Inc., Buffalo Grove, IL) and then imaged using a FEI Tecnai 12 Biospirit TEM (Hillsboro, OR) at 80 kV, at the Nanotechnology Innovation Center of Kansas State University (http://nicks.ksu.edu/electron-microscopy/). The bacteroid density and dimensions were determined by quantitative analysis of nodule TEM images using Adobe Photoshop software (Supporting Information).

### CNM Agglomeration in Soil Extracts

To understand how plant effects were related to CNM concentration-dependent agglomeration in moist soils, the short- and long-term stabilities of CNMs were studied in soil water extracts. Soil water extracts were prepared according to a published method with some modifications.[61] Briefly, control soil (Table S13) was weighed into separate 50 mL centrifuge tubes with 1:5 w/v (moist soil-to-water ratio) Nanopure water (Thermo Scientific Barnstead, Waltham, MA). The centrifuge tubes were sealed securely and shaken horizontally on a shaker for 3 h (25 °C, 250 rpm). The extract was centrifuged (3500 × g, 10 min) to separate large solids, and the supernatant was decanted. The supernatant was vacuum filtered through a 0.22 μm membrane filter (Millipore, Billerica, MA), and the filtrate was collected as the final soil extract and stored (−20 °C) prior to use.

A CNM stock solution (300 mg $L^{-1}$ ; Supporting Information) was prepared by weighing dry CNM powder into the filtered soil extract, then mixing by brief (5 min) sonication using a Branson 1510 bath sonicator (Branson Ultrasonics, Danbury, CT). Aliquots of the dispersed CNM stock solution were further diluted by the filtered soil extract to yield a final lower concentration of 10 mg $L^{-1}$. These two CNM concentrations (10 and 300 mg $L^{-1}$) were chosen for comparing the effect of lower versus higher CNM concentrations on CNM agglomeration in moist soil; both concentrations are relevant to the CNM doses used in the plant exposure experiment (Supporting Information). The CNM suspensions were bath-sonicated (5 min) immediately before use in static agglomeration and sedimentation studies, which were performed over a long time period (56 d). The changes of CNM hydrodynamic diameter and derived count rate[62] with time were measured using dynamic light scattering (DLS) in a Zetasizer NanoZS90 (Malvern Instruments Ltd., UK). DLS measurements were made every 15 s for the first 12 h, then daily from 1 to 7 d, and finally weekly until 56 d. Meanwhile, dynamic CNM sedimentation in the soil extract was monitored by measuring the suspension absorbance at 600 nm (as a proxy for suspended nanomaterial concentration[45,63]) using a UV-1800 spectrophotometer (Shimadzu, Japan). Sedimentation

patterns were inferred from the time course of normalized suspension absorbance at 600 nm (A/A0, where A0 was at time 0 of the experiment). The UV-1800 spectrophotometer was zeroed using Nanopure water. The absorbance (at 600 nm) of the filtered soil extract alone was monitored over time as well, to confirm there was no interfering absorbance from the soil extract in the CNM suspensions. The zeta (ζ) potential and electrophoretic mobility (EPM) of the filtered soil extract and of 10 mg $L^{-1}$ CNMs were also obtained using the Zetasizer NanoZS90. For either DLS, absorbance, ζ potential, or EPM, at least three replicate measurements were performed.

### Environmental Scanning Electron Microscopy of CNMs in the Soil Extract

Environmental scanning electron microscopy (ESEM) was performed to visualize the agglomerate morphologies of 10 and 300 mg $L^{-1}$ CNMs in the soil extract, against a clean quartz sand substrate. Specimens were prepared by dispensing approximately 100 μL of the CNM suspensions onto clean quartz sand (Accusand, Unimin Corp., New Canaan, CT) overlaying a 10 mm stainless steel conical-well Peltier stub. Imaging was by an FEI Co. XL30 field emission gun (FEG) microscope (Philips Electron Optics, Eindhoven, The Netherlands), operated at 15 kV accelerating voltage, in a 3.5-torr chamber pressure with a gaseous secondary electron detector (GSED) in environmental (wet) mode.

### Statistical Analyses

Data are shown as the mean ± SE (standard error). For each CNM type, one-way analysis of variance (ANOVA) with Tukey's or Games-Howell post hoc multiple comparisons was used to determine significant differences between treatments ($P < 0.05$). Homogeneity of variance was tested with Levene's test. To explore dose–response relationships, correlations were performed between plant growth and end point metrics with soil CNM concentrations, using both two-tailed linear and power regression models. Correlation analyses were conducted both with and without the control data. Statistical analyses were performed using Microsoft Excel 2013, IBM SPSS Statistics 23, and SigmaPlot 12.3.

## Supplementary Material

Refer to Web version on PubMed Central for supplementary material.

## Acknowledgments

This research was primarily funded by the National Science Foundation (NSF) and the Environmental Protection Agency (EPA) under Cooperative Agreement DBI-0830117. Any opinions, findings, and conclusions expressed in this material are those of the author(s) and do not necessarily reflect those of either the NSF or EPA. This work has not been subjected to EPA review, and no official endorsement should be inferred. Additionally, this research was supported in part by a Bren School Fellowship, a Mellichamp Academic Initiative in Sustainability Fellowship, and an Earth Research Institute Summer Fellowship to Y.W. We thank J. Priester, N. Rinaldi El-Abd, Z. Welch, M. Mortimer, P. Roehrdanz, M. Feraud, and Y. Ge for their assistance. S. Davis performed ESEM analysis in the Micro-Environmental Imaging and Analysis Facility at the University of California at Santa Barbara (http://www.bren.ucsb.edu/facilities/MEIAF/) under NSF Awards BES-9977772 and DBI-0216480. We acknowledge R. Thakkar at the Nanotechnology Innovation Center of Kansas State (http://nicks.ksu.edu/electron-microscopy/) for performing the TEM analysis of root nodules. We acknowledge the use of the Schuyler Greenhouse at the University of California at Santa Barbara, whose construction was funded by Dr. A. H. (Barry) and Jeanne Schuyler and NSF Grant OIA-0963547. We acknowledge the use of Sedgwick Natural Reserve in the University of California Natural Reserve System (http://www.ucnrs.org/). The MRL Shared Experimental Facilities are supported

by the MRSEC Program of the NSF under Award No. DMR 1121053, a member of the NSF-funded Materials Research Facilities Network (www.mrfn.org).

## References


1. De Volder MF, Tawfick SH, Baughman RH, Hart AJ. Carbon Nanotubes: Present and Future Commercial Applications. Science. 2013; 339:535–539. [PubMed: 23372006]
2. Zurutuza A, Marinelli C. Challenges and Opportunities in Graphene Commercialization. Nat Nanotechnol. 2014; 9:730–734. [PubMed: 25286257]
3. Nowack B, Ranville JF, Diamond S, Gallego-Urrea JA, Metcalfe C, Rose J, Horne N, Koelmans AA, Klaine SJ. Potential Scenarios for Nanomaterial Release and Subsequent Alteration in the Environment. Environ Toxicol Chem. 2012; 31:50–59. [PubMed: 22038832]
4. Petersen EJ, Zhang L, Mattison NT, O'Carroll DM, Whelton AJ, Uddin N, Nguyen T, Huang Q, Henry TB, Holbrook RD, Chen KL. Potential Release Pathways, Environmental Fate, and Ecological Risks of Carbon Nanotubes. Environ Sci Technol. 2011; 45:9837–9856. [PubMed: 21988187]
5. Keller AA, McFerran S, Lazareva A, Suh S. Global Life Cycle Releases of Engineered Nanomaterials. J Nanopart Res. 2013; 15:1692.
6. Pan B, Xing B. Applications and Implications of Manufactured Nanoparticles in Soils: A Review. Eur J Soil Sci. 2012; 63:437–456.
7. Gogos A, Knauer K, Bucheli TD. Nanomaterials in Plant Protection and Fertilization: Current State, Foreseen Applications, and Research Priorities. J Agric Food Chem. 2012; 60:9781–9792. [PubMed: 22963545]
8. Gardea-Torresdey JL, Rico CM, White JC. Trophic Transfer, Transformation, and Impact of Engineered Nanomaterials in Terrestrial Environments. Environ Sci Technol. 2014; 48:2526–2540. [PubMed: 24499408]
9. Mukherjee A, Majumdar S, Servin AD, Pagano L, Dhankher OP, White JC. Carbon Nanomaterials in Agriculture: A Critical Review. Front Plant Sci. 2016; 7:172. [PubMed: 26941751]
10. Rico CM, Majumdar S, Duarte-Gardea M, Peralta-Videa JR, Gardea-Torresdey JL. Interaction of Nanoparticles with Edible Plants and Their Possible Implications in the Food Chain. J Agric Food Chem. 2011; 59:3485–3498. [PubMed: 21405020]
11. Begum P, Ikhtiari R, Fugetsu B, Matsuoka M, Akasaka T, Watari F. Phytotoxicity of Multi-Walled Carbon Nanotubes Assessed by Selected Plant Species in the Seedling Stage. Appl Surf Sci. 2012; 262:120–124.
12. Begum P, Ikhtiari R, Fugetsu B. Graphene Phytotoxicity in the Seedling Stage of Cabbage, Tomato, Red Spinach, and Lettuce. Carbon. 2011; 49:3907–3919.
13. Servin AD, White JC. Nanotechnology in Agriculture: Next Steps for Understanding Engineered Nanoparticle Exposure and Risk. NanoImpact. 2016; 1:9–12.
14. Navarro E, Baun A, Behra R, Hartmann NB, Filser J, Miao AJ, Quigg A, Santschi PH, Sigg L. Environmental Behavior and Ecotoxicity of Engineered Nanoparticles to Algae, Plants, and Fungi. Ecotoxicology. 2008; 17:372–386. [PubMed: 18461442]
15. Gogos A, Moll J, Klingenfuss F, van der Heijden M, Irin F, Green MJ, Zenobi R, Bucheli TD. Vertical Transport and Plant Uptake of Nanoparticles in a Soil Mesocosm Experiment. J Nanobiotechnol. 2016; 14:40.
16. de Santiago-Martín A, Constantin B, Guesdon G, Kagambega N, Raymond S, Cloutier RG. Bioavailability of Engineered Nanoparticles in Soil Systems. J Hazard Toxic Radioact Waste. 2016; 20:B4015001.
17. Stampoulis D, Sinha SK, White JC. Assay-Dependent Phytotoxicity of Nanoparticles to Plants. Environ Sci Technol. 2009; 43:9473–9479. [PubMed: 19924897]
18. Holden PA, Schimel JP, Godwin HA. Five Reasons to Use Bacteria When Assessing Manufactured Nanomaterial Environmental Hazards and Fates. Curr Opin Biotechnol. 2014; 27:73–78. [PubMed: 24863899]

19. Ge Y, Priester JH, Mortimer M, Chang CH, Ji Z, Schimel JP, Holden PA. Long-Term Effects of Multiwalled Carbon Nanotubes and Graphene on Microbial Communities in Dry Soil. Environ Sci Technol. 2016; 50:3965–3974. [PubMed: 26962674]
20. Moll J, Gogos A, Bucheli TD, Widmer F, van der Heijden MG. Effect of Nanoparticles on Red Clover and Its Symbiotic Microorganisms. J Nanobiotechnol. 2016; 14:36.
21. Herridge DF, Peoples MB, Boddey RM. Global Inputs of Biological Nitrogen Fixation in Agricultural Systems. Plant Soil. 2008; 311:1–18.
22. Biswas B, Gresshoff PM. The Role of Symbiotic Nitrogen Fixation in Sustainable Production of Biofuels. Int J Mol Sci. 2014; 15:7380–7397. [PubMed: 24786096]
23. Sutton MA, Oenema O, Erisman JW, Leip A, van Grinsven H, Winiwarter W. Too Much of a Good Thing. Nature. 2011; 472:159–161. [PubMed: 21478874]
24. Priester JH, Ge Y, Mielke RE, Horst AM, Moritz SC, Espinosa K, Gelb J, Walker SL, Nisbet RM, An YJ, Schimel JP, Palmer RG, Hernandez-Viezcas JA, Zhao L, Gardea-Torresdey JL, Holden PA. Soybean Susceptibility to Manufactured Nanomaterials with Evidence for Food Quality and Soil Fertility Interruption. Proc Natl Acad Sci U S A. 2012; 109:E2451–E2456. [PubMed: 22908279]
25. Priester JH, Moritz SC, Espinosa K, Ge Y, Wang Y, Nisbet RM, Schimel JP, Susana Goggi A, Gardea-Torresdey JL, Holden PA. Damage Assessment for Soybean Cultivated in Soil with Either CeO2 or ZnO Manufactured Nanomaterials. Sci Total Environ. 2017; 579:1756–1768. [PubMed: 27939199]
26. Holden PA, Klaessig F, Turco RF, Priester JH, Rico CM, Avila-Arias H, Mortimer M, Pacpaco K, Gardea-Torresdey JL. Evaluation of Exposure Concentrations Used in Assessing Manufactured Nanomaterial Environmental Hazards: Are They Relevant? Environ Sci Technol. 2014; 48:10541–10551. [PubMed: 25158225]
27. Liu X, Gurel V, Morris D, Murray DW, Zhitkovich A, Kane AB, Hurt RH. Bioavailability of Nickel in Single-Wall Carbon Nanotubes. Adv Mater. 2007; 19:2790–2796.
28. Lin S, Reppert J, Hu Q, Hudson JS, Reid ML, Ratnikova TA, Rao AM, Luo H, Ke PC. Uptake, Translocation, and Transmission of Carbon Nanomaterials in Rice Plants. Small. 2009; 5:1128–1132. [PubMed: 19235197]
29. Khodakovskaya MV, Kim BS, Kim JN, Alimohammadi M, Dervishi E, Mustafa T, Cernigla CE. Carbon Nanotubes as Plant Growth Regulators: Effects on Tomato Growth, Reproductive System, and Soil Microbial Community. Small. 2013; 9:115–123. [PubMed: 23019062]
30. Takeno K. Stress-Induced Flowering: The Third Category of Flowering Response. J Exp Bot. 2016; 67:4925–4934. [PubMed: 27382113]
31. Tu JC. Rhizobial Root Nodules of Soybean as Revealed by Scanning and Transmission Electron Microscopy. Phytopathology. 1975; 65:447–454.
32. Huang YC, Fan R, Grusak MA, Sherrier JD, Huang CP. Effects of Nano-ZnO on the Agronomically Relevant Rhizobium–Legume Symbiosis. Sci Total Environ. 2014; 497–498:78–90.
33. Fan R, Huang YC, Grusak MA, Huang CP, Sherrier DJ. Effects of Nano-TiO2 on the Agronomically-Relevant Rhizobium–Legume Symbiosis. Sci Total Environ. 2014; 466–467:503–512.
34. Vesper SJ, Craig Weidensaul T. Effects of Cadmium, Nickel, Copper, and Zinc on Nitrogen Fixation by Soybeans. Water, Air, Soil Pollut. 1978; 9:413–422.
35. Imsande J. Interrelationship between Plant Developmental Stage, Plant Growth Rate, Nitrate Utilization and Nitrogen Fixation in Hydroponically Grown Soybean. J Exp Bot. 1988; 39:775–785.
36. Kapustka LA, Wilson KG. The Influence of Soybean Planting Density on Dinitrogen Fixation and Yield. Plant Soil. 1990; 129:145–156.
37. Wong PP, Evans HJ. Poly-β-Hydroxybutyrate Utilization by Soybean (Glycine max Merr.) Nodules and Assessment of Its Role in Maintenance of Nitrogenase Activity. Plant Physiol. 1971; 47:750–755. [PubMed: 16657699]
38. Ferguson BJ, Indrasumunar A, Hayashi S, Lin MH, Lin YH, Reid DE, Gresshoff PM. Molecular Analysis of Legume Nodule Development and Autoregulation. J Integr Plant Biol. 2010; 52:61–76. [PubMed: 20074141]

39. Redondo FJ, de la Pena TC, Morcillo CN, Lucas MM, Pueyo JJ. Overexpression of Flavodoxin in Bacteroids Induces Changes in Antioxidant Metabolism Leading to Delayed Senescence and Starch Accumulation in Alfalfa Root Nodules. Plant Physiol. 2009; 149:1166–1178. [PubMed: 19098093]
40. Chen C, Unrine JM, Judy JD, Lewis RW, Guo J, McNear DH Jr, Tsyusko OV. Toxicogenomic Responses of the Model Legume Medicago truncatula to Aged Biosolids Containing a Mixture of Nanomaterials (TiO2, Ag, and ZnO) from a Pilot Wastewater Treatment Plant. Environ Sci Technol. 2015; 49:8759–8768. [PubMed: 26065335]
41. Kiers ET, Rousseau RA, West SA, Denison RF. Host Sanctions and the Legume–Rhizobium Mutualism. Nature. 2003; 425:78–81. [PubMed: 12955144]
42. Judy JD, Unrine JM, Rao W, Wirick S, Bertsch PM. Bioavailability of Gold Nanomaterials to Plants: Importance of Particle Size and Surface Coating. Environ Sci Technol. 2012; 46:8467–8474. [PubMed: 22784043]
43. Wild E, Jones KC. Novel Method for the Direct Visualization of in Vivo Nanomaterials and Chemical Interactions in Plants. Environ Sci Technol. 2009; 43:5290–5294. [PubMed: 19708355]
44. Zhao S, Wang Q, Zhao Y, Rui Q, Wang D. Toxicity and Translocation of Graphene Oxide in Arabidopsis thaliana. Environ Toxicol Pharmacol. 2015; 39:145–156. [PubMed: 25499792]
45. Hyung H, Fortner JD, Hughes JB, Kim J-H. Natural Organic Matter Stabilizes Carbon Nanotubes in the Aqueous Phase. Environ Sci Technol. 2007; 41:179–184. [PubMed: 17265945]
46. Ji Z, Jin X, George S, Xia T, Meng H, Wang X, Suarez E, Zhang H, Hoek EM, Godwin H, Nel AE, Zink JI. Dispersion and Stability Optimization of TiO2 Nanoparticles in Cell Culture Media. Environ Sci Technol. 2010; 44:7309–7314. [PubMed: 20536146]
47. Ge Y, Priester JH, Van De Werfhorst LC, Walker SL, Nisbet RM, An YJ, Schimel JP, Gardea-Torresdey JL, Holden PA. Soybean Plants Modify Metal Oxide Nanoparticle Effects on Soil Bacterial Communities. Environ Sci Technol. 2014; 48:13489–13496. [PubMed: 25354168]
48. Horst AM, Neal AC, Mielke RE, Sislian PR, Suh WH, Madler L, Stucky GD, Holden PA. Dispersion of TiO2 Nanoparticle Agglomerates by Pseudomonas aeruginosa. Appl Environ Microbiol. 2010; 76:7292–7298. [PubMed: 20851981]
49. Perreault F, de Faria AF, Nejati S, Elimelech M. Antimicrobial Properties of Graphene Oxide Nanosheets: Why Size Matters. ACS Nano. 2015; 9:7226–7236. [PubMed: 26091689]
50. Kang S, Mauter MS, Elimelech M. Physicochemical Determinants of Multiwalled Carbon Nanotube Bacterial Cytotoxicity. Environ Sci Technol. 2008; 42:7528–7534. [PubMed: 18939597]
51. Liu S, Wei L, Hao L, Fang N, Chang MW, Xu R, Yang Y, Chen Y. Sharper and Faster "Nano Darts" Kill More Bacteria: A Study of Antibacterial Activity of Individually Dispersed Pristine Single-Walled Carbon Nanotube. ACS Nano. 2009; 3:3891–3902. [PubMed: 19894705]
52. Villagarcia H, Dervishi E, de Silva K, Biris AS, Khodakovskaya MV. Surface Chemistry of Carbon Nanotubes Impacts the Growth and Expression of Water Channel Protein in Tomato Plants. Small. 2012; 8:2328–2334. [PubMed: 22514121]
53. Lin C, Fugetsu B, Su Y, Watari F. Studies on Toxicity of MultiWalled Carbon Nanotubes on Arabidopsis T87 Suspension Cells. J Hazard Mater. 2009; 170:578–583. [PubMed: 19505757]
54. Holden PA, Gardea-Torresdey JL, Klaessig F, Turco RF, Mortimer M, Hund-Rinke K, Cohen Hubal EA, Avery D, Barcelo D, Behra R, Cohen Y, Deydier-Stephan L, Ferguson PL, Fernandes TF, Herr Harthorn B, Henderson WM, Hoke RA, Hristozov D, Johnston JM, Kane AB, et al. Considerations of Environmentally Relevant Test Conditions for Improved Evaluation of Ecological Hazards of Engineered Nanomaterials. Environ Sci Technol. 2016; 50:6124–6145. [PubMed: 27177237]
55. Screening Assessment for the Challenge. Carbon Black. Chemical Abstracts Service Registry Number 1333-86-4. Environment Canada, Health Canada; Canada: 2013. p. 20-31.
56. Kennedy AJ, Hull MS, Steevens JA, Dontsova KM, Chappell MA, Gunter JC, Weiss CA Jr. Factors Influencing the Partitioning and Toxicity of Nanotubes in the Aquatic Environment. Environ Toxicol Chem. 2008; 27:1932–1941. [PubMed: 19086318]
57. Mortimer M, Petersen EJ, Buchholz BA, Orias E, Holden PA. Bioaccumulation of Multiwall Carbon Nanotubes in Tetrahymena thermophila by Direct Feeding or Trophic Transfer. Environ. Sci Technol. 2016; 50:8876–8885.

58. Current Intelligence Bulletin 65: Occupational Exposure to Carbon Nanotubes and Nanofibers. National Institute for Occupational Safety and Health and Center for Disease Control; Atlanta, GA: 2013. p. 63

59. Pedersen, P. Soybean Growth and Development. University Extension, PM 1945, Iowa State University; Ames, IA: 2004. p. 3-18.Reviewed 2009

60. Weaver, RW., Danso, SKA. Dinitrogen Fixation. In: Bottomley, PS.Angle, JS., Weaver, RW., editors. Methods of Soil Analysis: Part 2-Microbiological and Biochemical Properties. Soil Science Society of America; Madison, WI: 1994. p. 1019-1045.

61. Jones D, Willett V. Experimental Evaluation of Methods to Quantify Dissolved Organic Nitrogen (DON) and Dissolved Organic Carbon (DOC) in Soil. Soil Biol Biochem. 2006; 38:991–999.

62. Shang J, Gao X. Nanoparticle Counting: Towards Accurate Determination of the Molar Concentration. Chem Soc Rev. 2014; 43:7267–7278. [PubMed: 25099190]

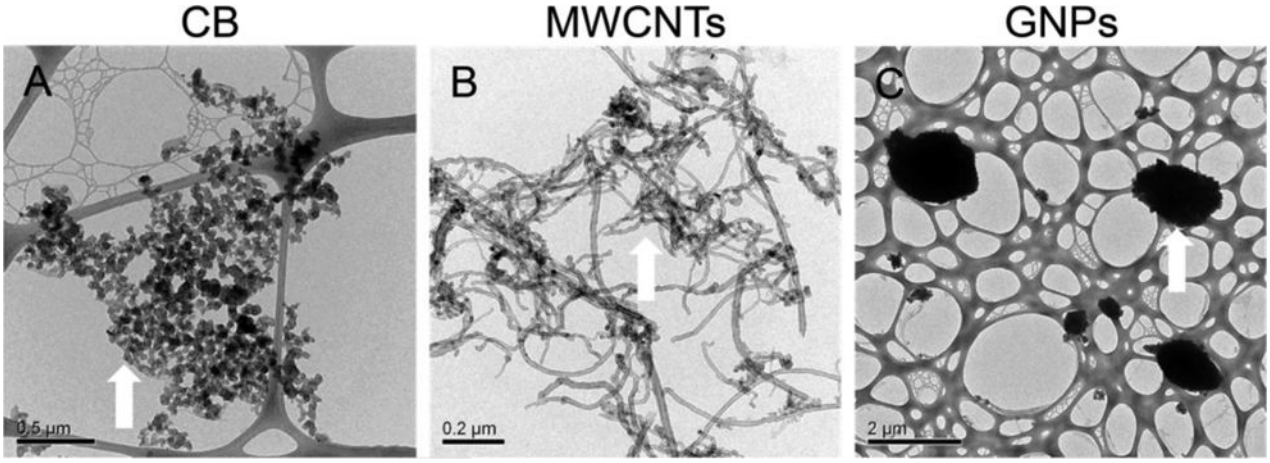


**Figure 1.**

Transmission electron microscopy (TEM) images of (A) carbon black (CB), (B) multiwalled carbon nanotubes (MWCNTs), and (C) graphene nanoplatelets (GNPs). White arrows indicate the representative features of corresponding nanomaterials. Scale bars are indicated in each image.

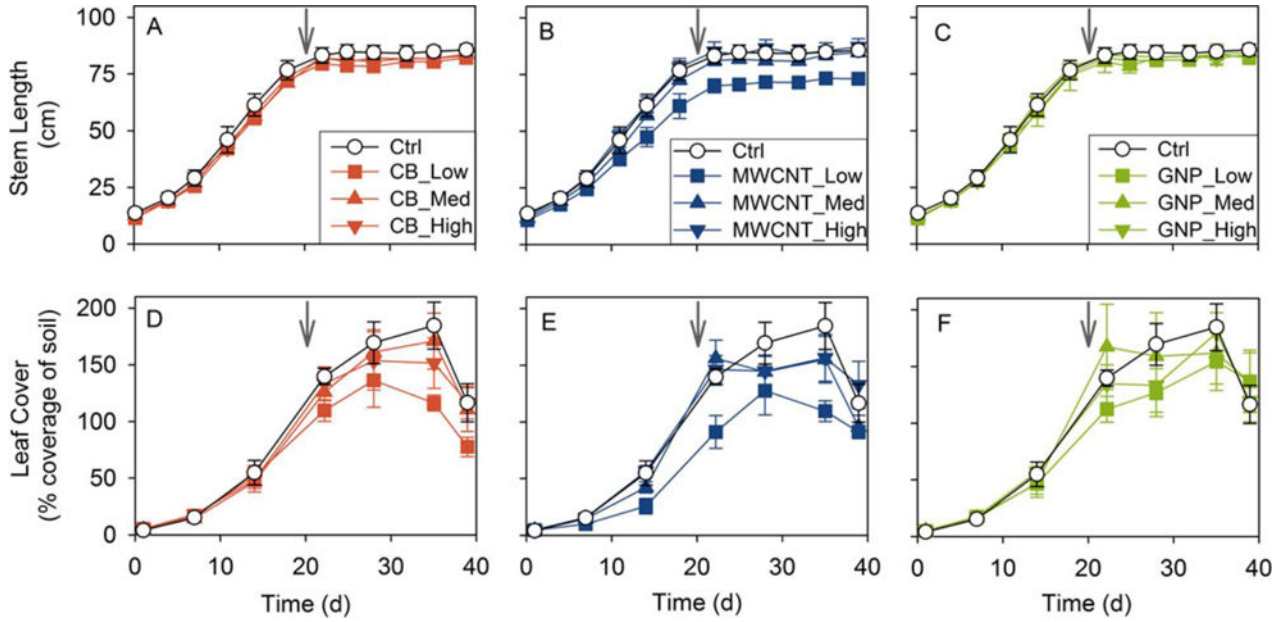


**Figure 2.**

Time course of soybean plant vegetative development post-transplantation according to either (A–C) stem length or (D–F) leaf cover (% coverage projected onto the pot soil surface). Ctrl = control without nanomaterial amendment, CB = carbon black, MWCNT = multiwalled carbon nanotubes, and GNP = graphene nanoplatelets. Low, med (medium), and high concentrations correspond to 0.1, 100, and 1000 mg $kg^{-1}$ nanomaterial on a dry soil basis. Gray arrows indicate when the intermediate harvest took place. Error bars are±SE (n = 5 plants, except n = 4 for the Ctrl, CB_High, and MWCNT_Low treatments).

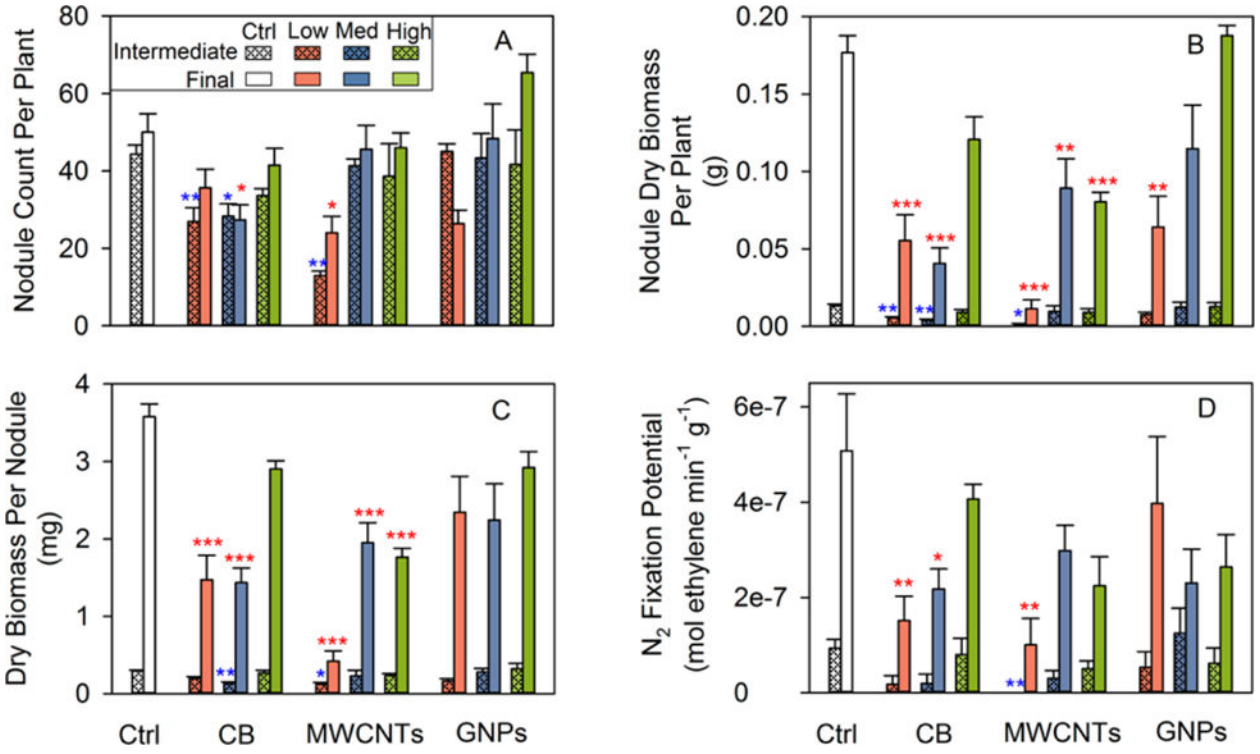


**Figure 3.**

Soybean root nodule production and N2 fixation potential according to treatment at the intermediate and final harvests, as measured by (A) nodule count per plant, (B) total nodule dry biomass per plant, (C) dry biomass per nodule, and (D) N2 fixation potential (normalized to dry nodule biomass). Ctrl = control without nanomaterial amendment, CB = carbon black, MWCNT = multiwalled carbon nanotubes, and GNP = graphene nanoplatelets. Low, med (medium), and high concentrations correspond to 0.1, 100, and 1000 mg $kg^{-1}$ nanomaterial on a dry soil basis. Error bars are ±SE (n = 3 plants at the intermediate harvest; n = 5 plants, except n = 4 for the Ctrl, CB_High, and MWCNT_Low treatments at the final harvest). *P < 0.05, **P < 0.01, and ***P < 0.001, as compared to the control (blue *, intermediate; red *, final).

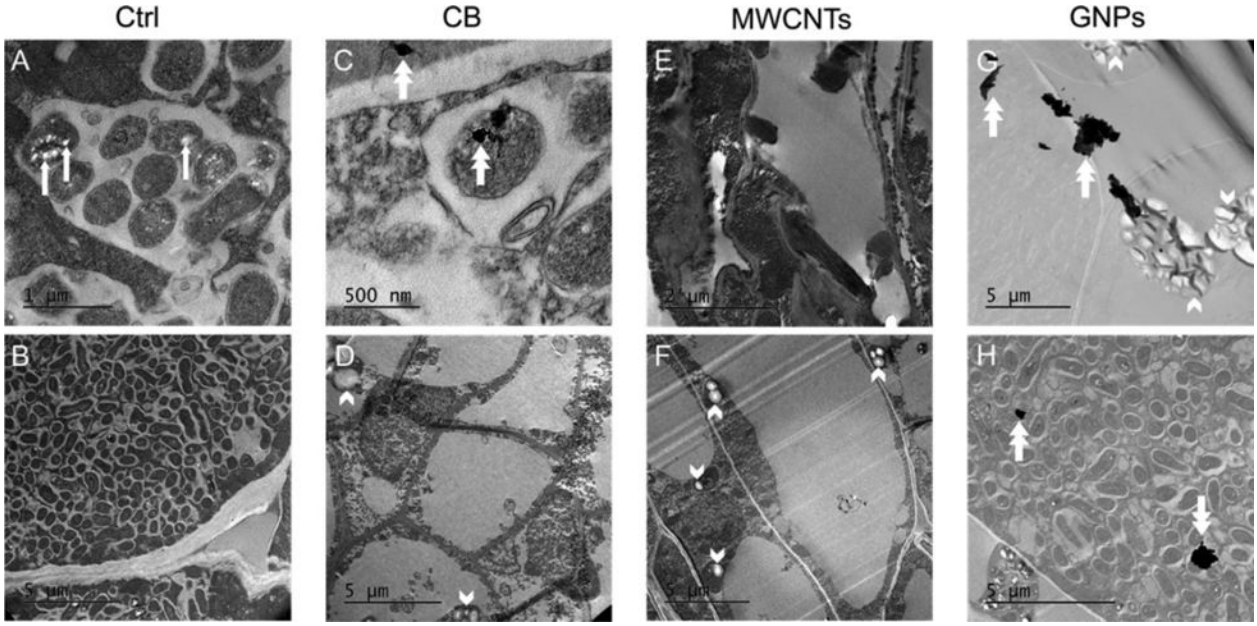


**Figure 4.**

Transmission electron microscopy (TEM) images of soybean root nodules at the final harvest from either (A, B) the controls (Ctrl), or the low exposures (0.1 mg $kg^{-1}$) of either (C, D) carbon black (CB), (E, F) multiwalled carbon nanotubes (MWCNTs), or (G, H) graphene nanoplatelets (GNPs). Scale bars are indicated in each image. Dense accumulations of bacteroids are evident in the Ctrl images at (A) high and (B) low magnifications. Within some bacteroids (e.g., Ctrl in part A), electron transparent (white-appearing) features (indicated by white arrows) are inferred to be poly(β-hydroxybutyrate) (PHB) inclusions. White double arrows point to apparent nanomaterials inside root nodule cells in the images for the CB (C) and GNP (G, H) treatments, only. The center double arrow in the CB image C indicates where nanomaterials appear associated with a bacteroid. Densely packed bacteroids are evident in one image (H) for the GNP treatment. Accumulations of putative starch granules (indicated by white arrowheads, external to bacteroids) are observed in the images for the CB (D), MWCNT (F), and GNP (G) treatments.

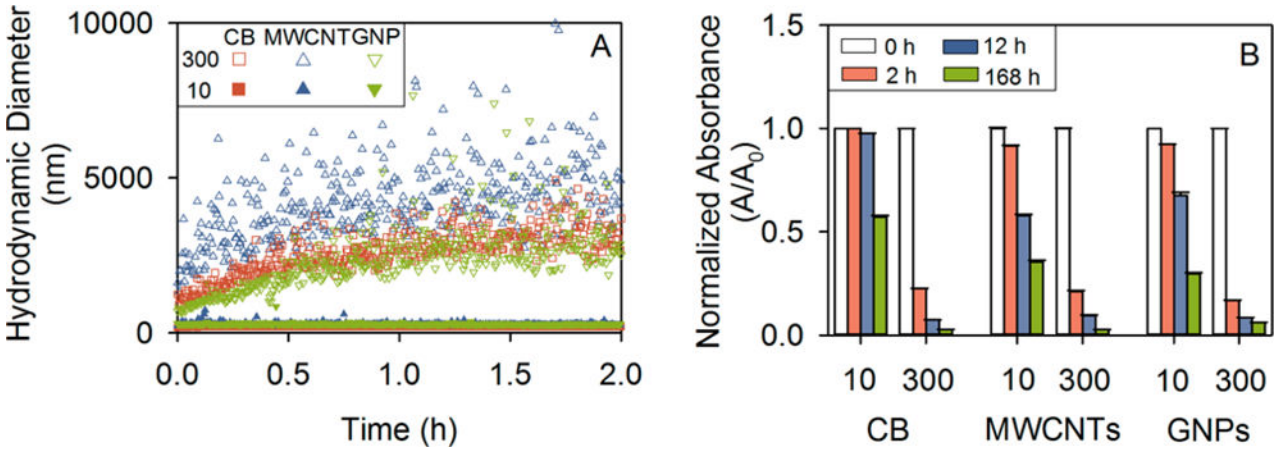


**Figure 5.**

Stability of either 10 or 300 mg $L^{-1}$ carbon black (CB), multiwalled carbon nanotubes (MWCNTs), or graphene nanoplatelets (GNPs) in the filtered soil extract as evidenced by (A) the early (first 2 h) time course of nanomaterial hydrodynamic diameter as measured by dynamic light scattering (DLS), and (B) the time course to 7 d of normalized nanomaterial suspension absorbance at 600 nm ($A/A_0$, where $A_0$ was at time 0 of the experiment; the suspension absorbance at 600 nm used as a proxy for suspended nanomaterial concentration). Error bars are ± SE (n = 3). Note that closed symbols in panel A are clustered along the ordinate for all CNMs at 10 mg $L^{-1}$, indicating that over the first 2 h of the stability assessment the hydrodynamic diameters of CNMs at 10 mg $L^{-1}$ were relatively low and constant.

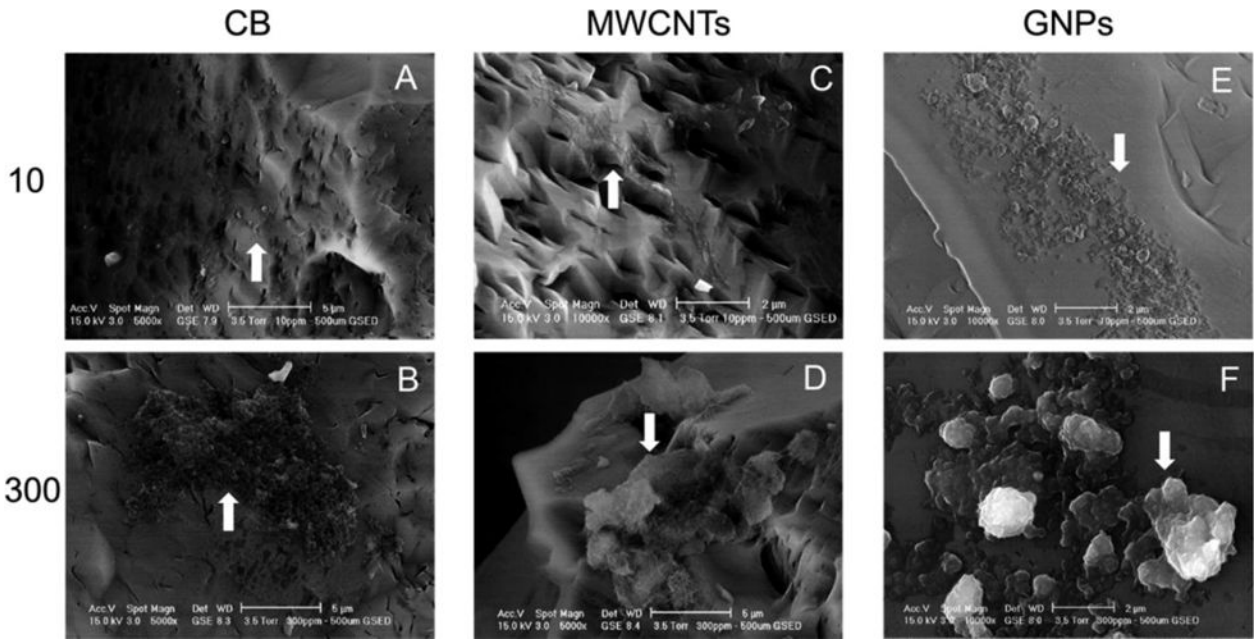


**Figure 6.**

Environmental scanning electron microscopy (ESEM) images of either 10 or 300 mg $L^{-1}$ (A, B) carbon black (CB), (C, D) multiwalled carbon nanotubes (MWCNTs), or (E, F) graphene nanoplatelets (GNPs) dispersed into the filtered soil extract then deposited onto clean quartz sand. Scale bars are either 5 (A, B, D) or 2 μm(C, E, F). White arrows indicate either dispersed nanomaterials at the lower concentration (10 mg$L^{-1}$; A, C, E) or larger nanomaterial agglomerates at the higher concentration (300 mg $L^{-1}$; B, D, F).

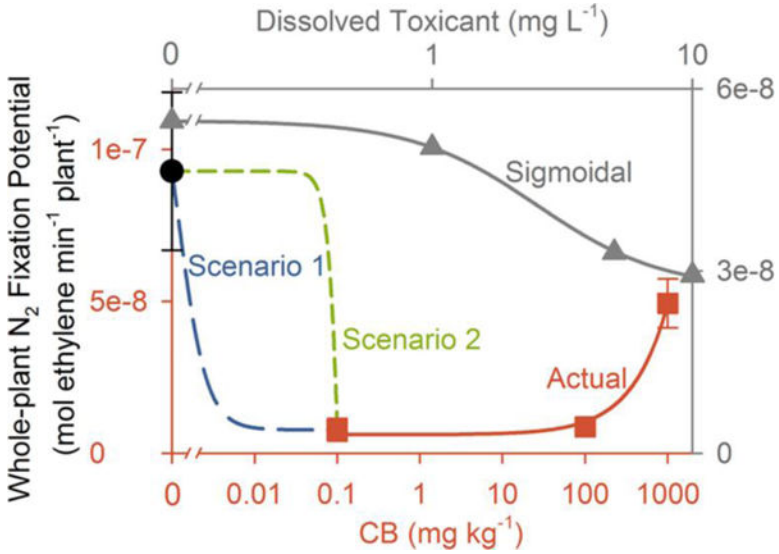


**Figure 7.**

Conceptual inverse dose–response relationship for an agglomerating, nondissolving nanomaterial that negatively affects soybean N2 fixation potential on a whole plant basis in moist soil. Results herein for carbon black (CB) exemplify observed data (actual, red squares connected by red solid lines, relative to red axes on the bottom and left; Table S11) for the tested CB doses of 0.1, 100, and 1000 mg $kg^{-1}$ dry soil at the final harvest. The black filled circle represents the observed control value (Table S11). Note the logarithmic scale of the x-axis for CB concentration. The whole-plant N2 fixation potential was reduced in all three CB treatments compared to the control but increased with CB concentration ($r = 0.90$, $P < 0.001$; Figure S6F). The gray solid line represents a sigmoidal dose–response curve for a toxicant that dissolves into the soil solution (with gray axes labeling on the top and right). This curve is based on data (gray triangles) generated by Vesper and CraigWeidensaul,[34] showing the effect of dissolved metal toxicant, copper, on soybean whole-plant N2 fixation potential measured by the acetylene reduction assay. Two alternative very low dose–response regimes are hypothesized. Scenario 1 (blue long dashed line) represents a continuum of responses between the control value and the lowest CB dose (0.1 mg $kg^{-1}$) tested herein. Scenario 2 (green short dashed line) represents a threshold dose, possibly close to the lowest dose (0.1 mg $kg^{-1}$) tested herein, below which CB inhibition of N2 fixation potential is not observed but above which it is. Although there is uncertainty in the untested low concentration regimes, this study supports that negative impacts are partly mitigated by CB agglomeration at the highest dose (1000 mg $kg^{-1}$).

## Table 1

Soybean Flower Count Per Plant at the Beginning of Reproduction[a]

| Treatment | Flower Count |
|---|---|
| Ctrl | 2.5 ± 1.0 |
| CB_Low | 5.8 ± 0.5* |
| CB_Med | 5.8 ± 0.7* |
| CB_High | 5.0 ± 0.4[b] |
| MWCNT_Low | 7.8 ± 1.8[c] |
| MWCNT_Med | 8.2 ± 1.1* |
| MWCNT_High | 8.2 ± 1.3* |
| GNP_Low | 9.6 ± 1.2** |
| GNP_Med | 11.8 ± 1.7*** |
| GNP_High | 10.4 ± 0.7** |

[a]Measured at day 22 post-transplantation (Figure S3). Ctrl = control without nanomaterial amendment, CB = carbon black, MWCNT = multiwalled carbon nanotubes, and GNP = graphene nanoplatelets. Low, med (medium), and high concentrations correspond to 0.1, 100, and 1000 mg $kg^{-1}$ nanomaterial on a dry soil basis. All data are shown as mean ± SE (n = 5 plants, except n = 4 for the Ctrl, CB_High, and MWCNT_Low treatments).

*P < 0.05,

**P < 0.01,

***P < 0.001, as compared to the control.

[b]P = 0.1

[c]P = 0.08, as compared to the control.